Journal of the Korean Physical Society
https://doi.org/10.1007/s40042-023-00841-7

Online ISSN 1976-8524
Print ISSN 0374-4884

ORIGINAL PAPER - FLUIDS, PLASMA AND PHENOMENOLOGY

Experimental design for observation of long beam-plasma instabilities

K. Moon[1] · J. Jeong[1] · C. Sung[1] · M. Chung[1]

Received: 9 January 2023 / Revised: 5 March 2023 / Accepted: 9 March 2023

Abstract
Depending on the electron beam parameters there can appear three beam-plasma instabilities which might be critical in beam-driven plasma wakefield accelerators. Those three instabilities are the self-modulation instability (SMI), hose instability (HI), and current filamentation instability (CFI) or for a long beam, oblique two-stream instability (OTSI), respectively. In majority of the cases, the classification of these instabilities is not clear unless any seed for an instability is given. As an experimental design, we suggest a simple switching method among the three instabilities by sweeping beam transverse emittance and radial size. Particularly, we investigate the mixed case of SMI and HI, and discuss the resonant condition of HI.

Keywords Self-modulation instability · Hose instability · Current filamentation instability · Cylindrical coordinates · Particle-in-cell simulation

1 Introduction

Ideas of plasma-based particle accelerators have been developed for decades with the promise of ultrahigh acceleration capability which is orders of magnitude higher than those of any conventional accelerators [1, 2]. Despite the great merit of this technology, many challenges have delayed its successful realization in the level of practical use [3–5]. They are not only technical issues that arise in the laboratory, but also theoretically inherent challenges. In plasma-based electron accelerators, the witness electrons, which are the target of acceleration, are supposed to be injected into the acceleration and focusing region of the plasma waves. The desired plasma wave is normally induced when the axisymmetric charged particle beam (or laser pulse) passes through the plasma [1, 2]. Therefore the stable propagation of driver beam in the plasma without any harmful instabilities has been one of the key issues in plasma-based electron accelerators.

Self-modulation instability (SMI) is well defined and developed with long ($k_p\sigma_z \gg 1$) and thin ($k_p\sigma_r \leq 1$) beam in over-dense plasma ($n_b/n_0 \ll 1$) [6], where k_p^{-1} is the collisionless plasma skindepth, σ_z the beam rms length, σ_r the beam rms radius, n_b the beam number density, and n_0 the ambient plasma number density, respectively. Since in long beam regime, Gaussian beam slices in longitudinal direction are distributed over several periods of the plasma wave, the net wakefields driven by the beam slices are averaged out. Thus effective SMI growth requires preceding seed wakefields [7]. The seed wakefield can be generated by a short preceding charged particle beam (or laser pulse) or sharply rising front of long beam (the beam rising time is on the order of k_p^{-1}/c) [8]. Transverse seed wakefield forces the beam envelope to be focused and defocused alternatively in the seed beam comoving frame $\xi = z - ct$, where c is the speed of light, t the propagation time of the beam in the plasma. This phenomenon has been actively studied for the last decade in the promise of using the proton beam of Super Proton Synchrotron (SPS) at CERN as a driver of beam driven plasma wakefield acceleration (BDPWFA) [9].

When driver beam is thin ($k_p\sigma_r < 1$), plasma electrons oscillate transversely, rapidly focusing the radial beam size. If the transverse phase spaces of beam or ambient plasma particles are initially asymmetric and beam particle's betatron motions are coherent in the phase and frequency, the centroids of beam slices oscillate and the amplitudes exponentially increase in ξ and t. In this case, the saturated radial beam size which is obtained by balancing focusing field and transverse beam emittance matters for the onset of hosing [10]. The betatron frequencies can be detuned by beam energy spread [4] and ξ dependence of wakefield

✉ M. Chung
mchung@unist.ac.kr

[1] Department of Physics, Ulsan National Institute of Science and Technology, Ulsan 44919, South Korea

Published online: 02 June 2023

amplitude [11]. The hosing of driver beam is one of the biggest concerns for stable operation of BDPWFA. Even though many theoretical and numerical expectations of hose instability (HI) have been proposed, yet they remain to be proved in laboratory.

When driver beam is wide ($k_p\sigma_r \gg 1$), plasma electrons which are pushed out by static field of driver beam mostly oscillate longitudinally, forming gently curved wakefield slope in radial direction [12]. In this case, the return current of plasma electrons pass through the driver beam body, inducing initially small turbulent magnetic field. If the Lorentz force is strong enough to guide beam particles against the transverse beam emittances $\epsilon_{x,y}$, the localized turbulent magnetic fields will modify orbits of beam and plasma particles. The modified orbits make anisotropy of beam distribution grow with transverse fields. As a result, the closed feedback loops of perturbations generate multiple current filaments. The detailed studies have shown that the actual onset condition is not exactly at $k_p\sigma_r \geq 1$, but the current filamentation instability (CFI), or for a long beam, oblique two-stream instability (OTSI) development also depends on the beam current and transverse emittances [5, 13, 14]. CFI has been studied with the great importance in the concept of magnetic field amplification and non-thermal particle acceleration at the steady state of relativistic unmagnetized shocks [15–17], but the effects of CFI on BDPWFA parameter regime applications have not been investigated enough yet.

Since three beam-plasma instabilities such as SMI, HI, and OTSI are all induced by the transverse dynamics of beam and plasma particles [5, 6, 10], the parameter regimes of these instabilities are not clearly classified. As an experiment design, we suggest a simple switching method among SMI, HI, and OTSI by sweeping beam transverse emittance and radial size. This work is based on electron beam parameter set from the Injector Test Facility (ITF) of Pohang Accelerator Laboratory (PAL) [18]. For the beamline and beam-plasma interaction simulations, the space charge tracking algorithm (ASTRA) [26] and quasi 3D particle-in-cell code (FBPIC) [20] were used.

2 Experiment setup

In order to experimentally study the various beam-plasma instabilities, the ITF at PAL is considered to be used. The facility has S-band RF guns, one of them is the coaxial coupled photocathode RF gun (GUN-II), which generate ~5 MeV electron beam by laser hitting the photocathode [21]. The initial beam parameters, normalized transverse emittance (NTE), and rms transverse beam size are determined by two variables such as laser intensity profile and magnetic fields from the gun solenoids. There are two parameters in laser intensity profile: the standard deviation of the laser distribution and the laser cut size by collimator. The generated electron beam is transported through the beamline, which includes RF booster cavity, quadrupole magnets, experimental chamber, deflecting cavity, dipole magnet, and diagnostic device in the sequence of Fig. 1. The target energy level in the range of 30–70 MeV is obtained by the booster cavity. By controlling the current on 3 quadrupole magnets after the booster cavity, we obtain the target rms beam radial sizes at the plasma entrance. Here, the quadrupole magnet triplet is supposed to affect only rms transverse beam size without influencing NTE. The expected ranges of electron beam parameters obtained from ASTRA simulations are: rms beam size 50–300 μm, NTE 1–10 mm-mrad, and relative rms energy spread 0.3%.

A custom-designed plasma source will be placed at the middle of GUN-II beam line shown in Fig. 1 [22]. The number density of pulsed DC discharge plasma is adjustable within the range $1.0 \times 10^{12} - 5.0 \times 10^{15}$ cm^{-3}. We first vacuum inside the tube connected to the gas line as shown in Fig. 2c on the order of 10^{-3} mbar. At the vacuum state, Argon gas is injected with the inner pressure of the tube on the order of 10^{-2} mbar. Argon gas is confined inside the

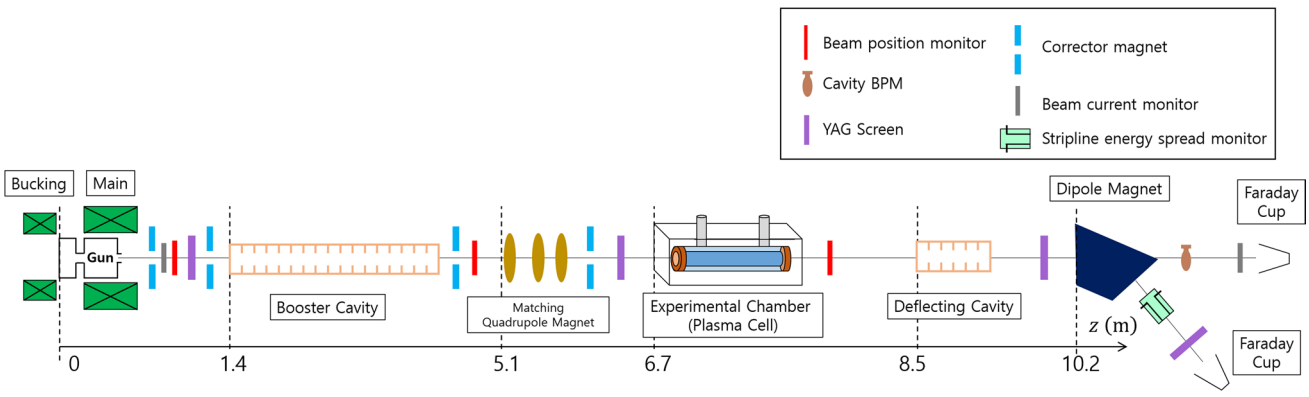

Fig. 1 Schematic of the ITF beamline (we note that recently the ITF has been renamed to eLABs: electron Linear Accelerator for Basic science)

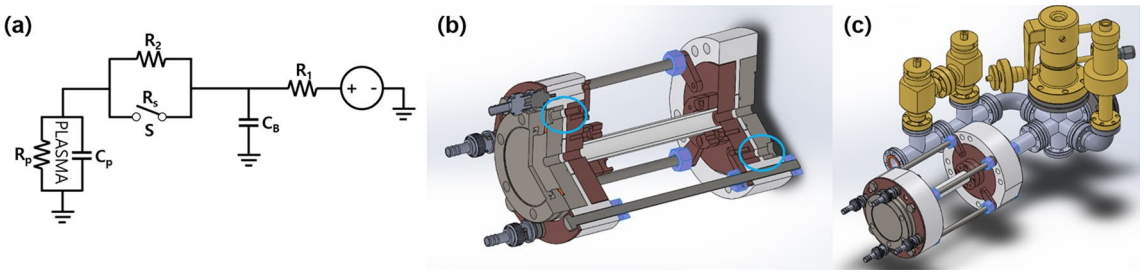

Fig. 2 **a** The switching circuit to control the currents in the plasma cell. S is the switch and C is the capacitor. R2 is the high-resistance resistor. **b** Plasma source structure. The inner structure (brown) is mainly composed of the electrodes. The left one is anode and the right one is cathode. They have M5 taps. Outer structure (grey) is modified blank flange, which has M5 holes. This structure is designed based on DN40 flange size ($D = 70$ mm). The inner and outer structures are divided by the PEEK insulator (white). **c** Plasma source with gas line system. From the left, clockwise: angle valves, gas valve, and pressure gauge. Argon is injected from the gas valve, and the total gas flow toward the vacuum pump is controlled by the two angle valves. Pressure is measured by the gauge near the 6-way cross

glass tube by installing thin polymer metal foils at both ends of the plasma cell [23] in Fig. 2b. The foil windows block the Argon gas particles, while allowing the electron beam passing through. The material is polyethylene terephthalate (PET) with Aluminum coating. Gas permeation constant of this film is lower than 10^{-13} m^2/s. The film scatters 23 MeV electron beam within very small angle 0.1–0.2 mrad at the film thickness 0.9–1.9 μm [24]. Since the vacuum pump will be working at the same time, Argon gas continuously flows and the system remains in a constant pressure. Once the pressure is stabilized, DC high voltage is applied to the electrodes with low current, generating glow discharge in the glass tube. The current control for triggering the arc discharge plasma is made by the switching circuit illustrated in Fig. 2a [23]. The circuit has two modes: glow discharge mode with switch-off and arc discharge mode with switch-on. When the switch is off, the current flows toward the plasma source by passing the high resistance resistor R2, while the charge is accumulated in the capacitor C. When the switch is on, the charge in the capacitor flows through the switch S owing to the lower resistance of switch S, initiating the high-peak-current arc discharge in the tube.

The plasma source has the mechanical structure depicted in Fig. 2b. The distance between the electrodes (or the length of the glass tube with 10 mm inner diameter) can be easily adjusted by using different length of the glass tube in the range of 100–200 mm. Once the plasma is generated, the charge is guided from the anode to the 4 bolt columns, and pass the BNC outer cable, then finally get dumped into the ground. While generating arc discharge plasma, the high voltage electrodes are isolated from the beam and gas lines by PEEK insulator [25]. The white structure in Fig. 2b which covers the brown electrodes is the PEEK holder with the dielectric strength of ~20 kV/mm and the thickness of 3 mm at the cylindrical center. The outer flanges are connected to the electrodes by the PEEK bolts marked by the blue circles in Fig. 2b.

After the beam passes through the plasma, dipole magnet (or deflecting cavity) will be used for steering the electron beam before the measurement device such as YAG screen (or Faraday cup), which will provide us the resultant beam information after the beam-plasma interaction at the end of the beam line.

3 Instability classification by beam radial size and transverse emittance

We performed simulation study with a flattop electron beam which is made by stacking eight short Gaussian pulses. The flattop beam initial parameters are the rms length $L_b/c = 8$ ps, the head length $\Delta L_b/c = 0.8$ ps, the rms radius $\sigma_r = 100 - 300$ μm, the normalized transverse emittance $\epsilon_r = 1 - 15$ μm, the total charge $Q_b = 200$ pC, and the mean relativistic gamma $\langle \gamma_b \rangle = 60$. The plasma density profile at the entrance is the step function. The ambient plasma density is $n_0 = 1 - 2.0 \times 10^{16}$ cm^{-3}. The flattop beam has a linear tilt of the beam transverse centroid $x_c/L_b = 9.3 \times 10^{-3}$ which works as a seed of HI. Numerical parameters are set to be spatial grids $k_p \Delta z = k_p \Delta r = 0.04$, number of azimuthal modes $N_m = 5$, number of plasma macro particles in each direction $N_z = N_r = 2$, $N_\phi = 4(N_m - 1) = 16$, number of beam macro particles $N_{bm} = 8 \times 10^6$, sizes of simulation box in each direction $R_{\rm box} = 1.5$ mm and $Z_{\rm box} = 3$ mm, respectively. Positions and momenta of beam macro particles are randomly generated by normal distribution generator which causes intrinsic statistical noise.Truncation of azimuthal modes in cylindrical coordinates makes the simulation cheaper by orders of magnitude compared to full 3D simulation [20]. Even though the azimuthal mode convergence tests show that the pattern of current filamentation differs with the

number of azimuthal modes, the onset of OTSI is observed equivalently in every number of azimuthal modes. Yet it is not clear if the cylindrical coordinate system can imitate all qualitative features of OTSI in full 3D system or not.

Figure 3 shows classification of a long beam-plasma instability by beam radial size and transverse emittance. The flattop electron beam has a tilt for HI seeding in every case and the beam rising time is short enough to generate considerable seed wakefield for SMI. When $\sigma_r = 100\ \mu$m and $\epsilon_r = 1$ mm-mrad, the transverse centroids of tilted beam are mismatched with those of wakefields which were generated by a sharply rising beam front and the fields are strong enough to guide the relativistic beam particles against the beam emittance. The mismatching of beam and wakefield transverse centroids causes hosing of the long flattop electron beam after the propagation distance of 20 cm (Fig. 3d). When $\sigma_r = 300\ \mu$m and $\epsilon_r = 1$ mm-mrad, the mismatching of beam and wakefield centroids is negligible. Instead, the magnetic field from the beam-plasma current enhances the anisotropy of the current distribution. Figure 3f shows that the field energy increase by OTSI is negligible in linear regime. The field energy increase in our regime is dominated by the beam betatron motion. It means whether the OTSI in linear regime can grow or not is determined solely by the betatron frequency from the beam driven plasma wakefield. When $\epsilon_r > 10$ mm-mrad, the electromagnetic fields from the statistical noise are negligible. The plasma wakefield driven by the beam front is dominant in Fig. 3b, c, and e. Figure 3 shows that SMI is most endurable to and OTSI is most easily suppressed by the large beam emittance. Since the current filamentation of the beam requires very low emittance and the filaments easily emerge after the plasma [5], rather we focus on the border of the onset of SMI and HI, which appears ambiguous in Fig. 3b, c, and e.

4 Resonant condition of long beam hosing

Over last 10 years, SMI and HI have been intensively studied together in the perspective of which one would grow faster in what condition. The confirmed statements are that the onset condition of long beam hosing is determined by the sizes and the tilt of the beam [7, 10], the envelope modulation in over-dense plasma widens the bandwidth of beam betatron frequency and detunes the resonant growth of hosing [10], and the long beam envelope modulation and centroid displacement equations are coupled [19]. One can assume that for the envelope modulation to increase the amplitude of the centroid displacement, two instabilities should be matched at the specific phase.

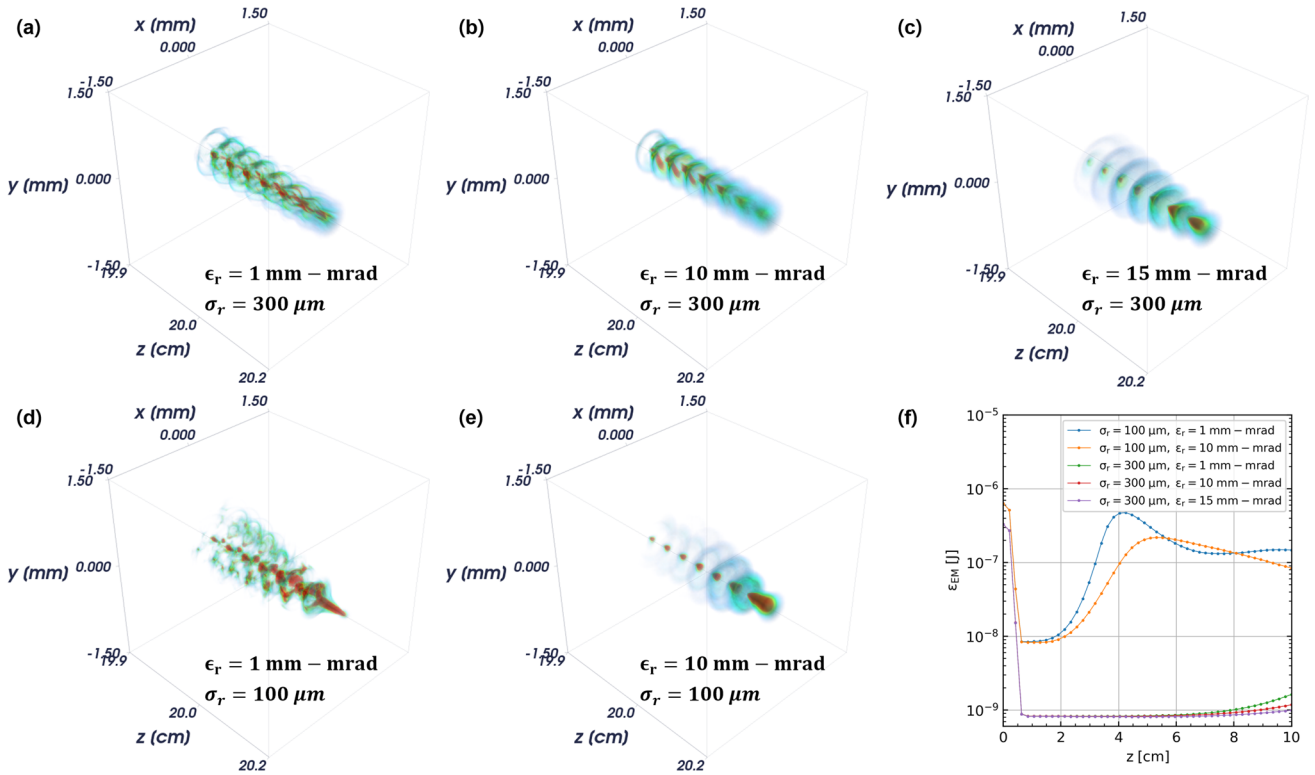

Fig. 3 Classification of beam-plasma instabilities by beam radial size and transverse emittance. The flattop electron beam has a tilt in every case. **a** OTSI, **b** and **d** HI-SMI mixed mode, and **c** and **e** pure SMI at $z = 20$ cm. **f** Their integrated field energies in propagation distance

The seeds of SMI and HI are from the sharply rising beam front and the tilt, respectively. The phase of SMI seed can be analytically estimated by the equation of beam driven plasma wakefield in linear regime. On the other hand, how to estimate the phase of hosing seed has not been reported in detail. Figure 4a–e show the qualitative transition of the long flattop beam-plasma instability with increasing ambient plasma density n_0. The initial beam rms radial size is $\sigma_r = 50\ \mu$m, the normalized emittance $\epsilon_r = 1\ \mu$m, the linear tilt $x_c/L_b = 1.9 \times 10^{-3}$, and other parameters are same as the ones in the previous section. In Fig. 4a, the beam envelope modulation and the centroid displacement are mixed in a beam. The beam front-driven plasma wakefield makes the microbunches at the focusing phase, while the beam is suffering from the centroid displacement instability at the defocusing phase. The red curve shows the beam current within $r < k_{pe}^{-1}$. In Fig. 4e,

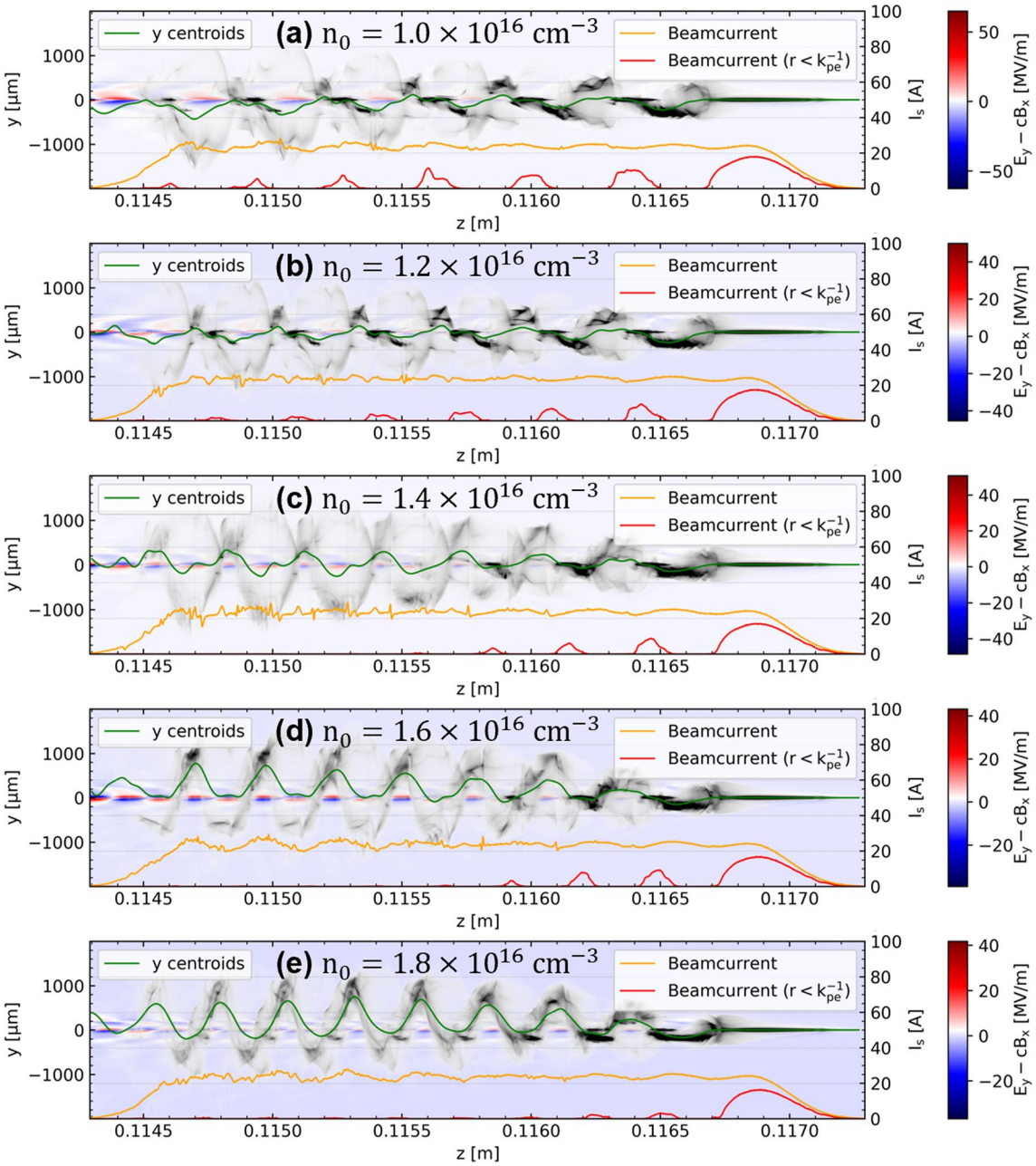

Fig. 4 Qualitative transition of the long flattop electron beam-plasma instability with varying ambient plasma number density n_0 at $z \approx 11$ cm. (grey shades) 2D distributions of the beam. (green curves) Transverse (or vertical) centroids of the beam. (orange curves) Total beam currents. (red curves) Beam currents near the propagation axis ($r < k_{pe}^{-1}$)

envelope focusing happens at the phase where the centroid displacement is at the crest. In the case, the beam current on the axis ($r < k_{pe}^{-1}$, red curve) is negligible. Overview of Fig. 4a–e tells us that the phases of SMI and HI seeds can be matched or mismatched. When the phases of the seeds are mismatched, two instabilities are mixed. When the phases of the seeds are matched, the long charged particle beam purely suffers from hosing, the centroid displacement instability.

5 Conclusions

In order to manipulate the type of long beam-plasma instabilities such as SMI, HI, and OTSI, we performed PIC simulations sweeping beam transverse emittance and radial size. We used flattop electron beam stacked by eight short Gaussian pulses. The instability appears as OTSI for wide and low emittance beam, SMI-HI mixed mode for thin and low emittance beam, and pure SMI for high emittance beam. The SMI-HI mixed case is from the mismatched phases of the instability seeds. The plasma source has been built for the purpose of performing the experiment at Injector Test Facility of Pohang Accelerator Laboratory.

Acknowledgements This work was supported by the National Research Foundation of Korea (Grants No. NRF-2016R1A5A1013277 and NRF-2020R1A2C1010835).

References

1. P. Chen, J.M. Dawson, R.W. Huff, T. Katsouleas, Acceleration of electrons by the interaction of a bunched electron beam with a plasma. Phys. Rev. Lett. **54**, 7 (1985)
2. T. Tajima, J.M. Dawson, Laser electron accelerator. Phys. Rev. Lett. **43**, 4 (1979)
3. X.L. Xu, J.F. Hua, Y.P. Wu, C.J. Zhang, F. Li, Y. Wan, C.H. Pai, W. Lu, W. An, P. Yu, M.J. Hogan, C. Joshi, W.B. Mori, Preservation of beam emittance in the presence of ion motion in future high-energy plasma-wakefield-based colliders. Phys. Rev. Lett. **104**, 155001 (2010)
4. T.J. Mehrling, R.A. Fonseca, A. Martinez de la Ossa, J. Vieira, Mitigation of the hose instability in plasma-wakefield accelerators. Phys. Rev. Lett. **118**, 174801 (2017)
5. B. Allen, V. Yakimenko, M. Babzien, M. Fedurin, K. Kusche, P. Muggli, Experimental study of current filamentation instability. Phys. Rev. Lett **109**, 185007 (2012)
6. N. Kumar, A. Pukhov, Self-modulation instability of a long proton bunch in plasma. Phys. Rev. Lett. **104**, 255003 (2010)
7. C.B. Schroeder, C. Benedetti, E. Esarey, F.J. Grüner, W.P. Leemans, Coherent seeding of self-modulated plasma wakefield accelerators. Phys. Plasmas **20**, 056704 (2013)
8. Y. Fang, V.E. Yakimenko, M. Babzien, M. Fedurin, K.P. Kusche, R. Malone, J. Vieira, W.B. Mori, P. Muggli, Seeding of self-modulation instability of a long electron bunch in a plasma. Phys. Rev. Lett. **112**, 045001 (2014)
9. E. Adli et al., Experimental observation of proton bunch modulation in a plasma at varying plasma densities. Phys. Rev. Lett. **122**, 054802 (2019)
10. J. Vieira, W.B. Mori, P. Muggli, Hosing instability suppression in self-modulated plasma wakefields. Phys. Rev. Lett. **112**, 205001 (2014)
11. A. Martinez de la Ossa, T.J. Mehrling, J. Osterhoff, Intrinsic stabilization of the drive beam in plasma-wakefield accelerators. Phys. Rev. Lett. **121**, 064803 (2018)
12. J.J. Su, T. Katsouleas, J.M. Dawson, P. Chen, M. Jones, R. Kening, Stability of the driving bunch in the plasma wakefield accelerator. *IEEE Trans. Plasma Sci.*, PS-15, 2 (1987)
13. N. Shukla, J. Vieira, P. Muggli, G. Sarri, R. Fonseca, L.O. Silva, Conditions for the onset of the current filamentation instability in the laboratory. J. Plasma Phys. **84**, 905840302 (2018)
14. P. San Miguel Claveria et al., Spatiotemporal dynamics of ultrarelativistic beam-plasma instabilities. Phys. Rev. Res. **4**, 023085 (2022)
15. A. Spitkovsky, Particle acceleration in relativistic collisionless shocks: Fermi process at last? Astrophys. J. **682**, L5 (2008)
16. S.F. Martins, R.A. Fonseca, L.O. Silva, W.B. Mori, Ion dynamics and acceleration in relativistic shocks. Astrophys. J. **695**, L189 (2009)
17. G.F. Swadling, C. Bruulsema, F. Fiuza, D.P. Higginson, C.M. Huntington, H.-S. Park, B.B. Pollock, Measurement of kinetic-scale current filamentation dynamics and associated magnetic fields in interpenetrating plasmas. Phys. Rev. Lett. **124**, 215001 (2020)
18. H.S. Kang et al., PAL-XFEL technical design report. *Pohang Accelerator Laboratory (Rev. ed.), 99-119* (2012)
19. C.B. Schroeder, C. Benedetti, E. Esarey, F.J. Grüner, W.P. Leemans, Coupled beam hose and self-modulation instabilities in overdense plasma. Phys. Rev. E **86**, 026402 (2012)
20. R. Lehe, M. Kirchen, I.A. Andriyash, B.B. Godfrey, J.-L. Vay, A spectral, quasi-cylindrical and dispersion-free particle-in-cell algorithm. Comput. Phys. Commun. **203**, 66–82 (2016)
21. J. Hong et al., Performance of S-band photocathode RF gun with coaxial coupler. in *Proceedings of the 39th Free Electron Laser Conference (FEL'19), Hamburg, Germany, 26-30 August 2019*. JACOW Publishing, Geneva, Switzerland (2019)
22. J.H. Han et al., Beam operation of the PAL-XFEL injector test facility. in *Proceedings of the 36th Free Electron Laser Conference (FEL'14), Basel, Switzerland, 25-29 August 2014*. JACOW Publishing, Geneva, Switzerland (2014)
23. Gregor Loisch, *Demonstrating High Transformer Ratio Beam-Driven Plasma Wakefield Acceleration*. PhD thesis, Staats-und Universitätsbibliothek Hamburg Carl von Ossietzky, 74–76 (2019)
24. O. Lishilin et al., First results of the plasma wakefield acceleration experiment at PITZ. Nucl. Instr. Methods Phys. Res. A **16**(041301), 37–42 (2016)
25. D.K. Das-Gupta, K. Doughty, Dielectric and conduction processes in polyetherether ketone (PEEK). IEEE Trans. Electr. Insulation **1**, 1–7 (1987)
26. K. Floettmann, ASTRA: A Space Charge Tracking Algorithm. *DESY*, v3.2 (2017)